European Journal of Pharmaceutics and Biopharmaceutics 214 (2025) 114804

Contents lists available at ScienceDirect

European Journal of Pharmaceutics and Biopharmaceutics

journal homepage: www.elsevier.com/locate/ejpb

Research paper

Stimuli-sensitive hyaluronic acid hydrogels for localized and controlled release of antibodies

Bita Mahdavi Firouzabadi [a], Maria Rosa Gigliobianco [b], Dimitrios Agas [c], Maria Giovanna Sabbieti [c], Claudio Alimenti [c], Lakshmi Sathi Devi [a], Cristina Casadidio [a,*], Piera Di Martino [b], Roberta Censi [a]

[a] School of Pharmacy, University of Camerino, ChIP Chemistry Interdisciplinary Project Research Centre, Via Madonna delle Carceri, 62032 Camerino, MC, Italy
[b] Department of Pharmacy, "G. D'Annunzio" Chieti e Pescara University, Via dei Vestini 1, 66100 Chieti, CH, Italy
[c] School of Biosciences and Veterinary Medicine, University of Camerino, Via Gentile III da Varano, 62032 Camerino, MC, Italy

ARTICLE INFO

Keywords:
Immunoglobulins
Redox-sensitive
Drug delivery
Immunotherapy
Polysaccharide

ABSTRACT

Stimuli-sensitive hydrogels are utilized in therapeutic applications for their ability to function as controlled drug delivery systems, particularly as delivery platforms for antibodies in cancer treatment. Their adaptive properties, including biocompatibility, high water retention, and tunable mechanical strength, make them well-suited for local and sustained drug release. In this study, redox-sensitive hydrogels based on thiolated hyaluronic acid (HA-SH) were synthetized as tunable platforms for controlled antibody delivery in cancer therapy. HA-SH hydrogels with different degrees of substitution (DS30, DS50 and DS70) exhibited distinct structural and mechanical properties, with HA-SH DS70 forming a denser network and demonstrating greater stability compared to HA-SH DS30 and DS50. Swelling and degradation studies confirmed redox responsiveness of the gels, with DS30 gel degrading faster than DS50 and DS70 gels in reductive environments. Rheological analysis further showed that higher cross-linking density in DS70 gels enhanced viscosity and mechanical strength compared to DS50 and DS30. Immunoglobulin G (IgG), used as a model drug for immunotherapeutic agents, was loaded into DS30 and DS70 hydrogels. The release followed zero-order kinetics at pH 7.4, highlighting the influence of the polysaccharide intrinsic anionic properties. DS30 hydrogels demonstrated sustained release (85 ± 6 % in 9 days), while DS70 exhibited faster release (71 ± 7 % in 5 days). The IgG release kinetics relied on a dual mechanism involving the combination of gel erosion (depending on DS and structural features), as well as IgG poly-charged nature and its ionic interactions with the hyaluronic acid polymeric network, as highlighted by rheological measurements and differential scanning calorimetry (DSC) analysis. Overall, the study highlights the potential of HA-SH hydrogels as customizable and localized immunotherapeutic delivery systems for controlled and precise cancer treatment.

1. Introduction

Hydrogels, characterized by their three-dimensional polymeric networks with flexible structures and biocompatible characteristics, have gained significant attention, particularly in the field of cancer immunotherapy [1]. Their hydrophilic and flexible nature makes hydrogels ideal platforms for entrapping immunotherapeutic agents, preserving their natural structure in a viscoelastic network, saving them from premature degradation by body fluids and enzymes, meanwhile reducing the need for high-dosage administration [2,3]. For these reasons, hydrogels are under investigation in several clinical trials as suitable carriers for many biopharmaceuticals and immune cells, presenting promising prospects for personalized medicine [4,5].

One of the most important applications of hydrogels is as a platform for the delivery of immunotherapeutic agents such as immune stimulatory cytokines and monoclonal antibodies. Currently, the majority of clinically used therapeutic antibodies are immunoglobulin G (IgG) monoclonal antibodies [6]. Cancer immunotherapy, either by activating immune responses using vaccine platforms or by passive immune system stimulation through antibody injection, needs an infrastructure that provides and accelerates the adhesion, traffic, and function of immune cells [7]. Therefore, hydrogels offer convenient systems for the delivery

* Corresponding author.
E-mail address: cristina.casadidio@unicam.it (C. Casadidio).

https://doi.org/10.1016/j.ejpb.2025.114804
Received 23 November 2024; Received in revised form 30 May 2025; Accepted 7 July 2025
Available online 8 July 2025

of immunotherapeutic agents.

Hydrogels possess meshed space amongst the polymer chains that allow nutrients and small molecules to pass through, preserving the structural and chemical stability of the payload while providing a biocompatible interface with living tissues. Therefore, hydrogels are considered as one of the optimal systems for the delivery of biopharmaceuticals, which, in contrast to small molecule drugs, often have large structures. The mesh size can differ based on the concentrations of polymers and cross-linkers, as well as external stimuli such as temperature, redox species, and pH [8,9]. Drug release is controlled by factors such as swelling and degradation rate, crosslinking density, polymer concentration, and the interactions between biomolecules. Various tailored drug delivery systems can be designed by adjusting the chemical properties of the hydrogels to be responsive to specific conditions and triggers, such as pH changes or enzymatic activity [10]. For cancer therapy, it is crucial to consider the properties of the tumor microenvironment (TME). The TME exhibits specific characteristics distinct from normal physiological conditions including low pH, hypoxia, and redox imbalances. These distinctive conditions can be utilized in developing drug delivery systems specifically designed to reach and treat tumors effectively [11].

Hyaluronic acid is a natural polysaccharide and one of the most abundant components in the extracellular matrix (ECM) [12,13]. It has been widely used in hydrogel studies due to its promising properties such as biocompatibility, biodegradability, and non-antigenicity [14]. Due to these intrinsic features, hyaluronic acid-based hydrogels are increasingly studied as drug delivery systems, especially in cancer treatment [15,16]. However, hyaluronic acid in its native form is not capable of forming hydrogels with desirable physicochemical properties, necessitating chemical modifications to its primary structure for optimal biomedical applications [17,18]. Thiolation of hyaluronic acid is considered an optimal strategy, as the crosslinking between polymeric chains during hydrogel formation occurs via disulfide bonds, which are degradable in the redox environment, such as the TME [19–21]. This approach enables the creation of stimuli-sensitive hydrogels capable of adapting to environmental changes.

In this study, novel thiolated hyaluronic acid-based hydrogels with varying degrees of substitution (DS30, DS50 and DS70) were prepared and systematically characterized, focusing on their morphological and rheological properties, as well as their swelling and degradation behavior. The incorporation of disulfide bond formation facilitated *in situ* crosslinking of the hydrogels, offering an innovative method for modulating the gels structural and mechanical properties. For the first time, the interactions between IgG and hyaluronic acid within these hydrogel matrices were explored, investigating their potential as immunotherapeutic tailorable delivery systems. Experiments were conducted to examine the loading and subsequent release of IgG, providing insights into how the specific chemical features of the hydrogels influence the release mechanism. This investigation considered not only the crosslinking density but also the hydrogel charge density, which is inherently dependent on crosslinking, as variations in crosslinking naturally alter the distribution of ionic groups within the polysaccharidic hydrogel network. Thermal analysis and rheological measurements were employed to highlight these interactions further. *In vitro* cytocompatibility studies were carried out to evaluate the safety and biocompatibility of the hydrogels, supporting their potential for future applications as customizable delivery platforms for immunotherapeutic agents.

2. Materials and Methods

2.1. Materials

Unless stated otherwise, all chemicals were purchased from Sigma Aldrich (Stenheim, Germany) and used as received. Sodium hyaluronic acid (Mw = 38 kDa) was purchased from Lifecore, Biomedical (Chaska, USA). Ultrapure water was produced in the laboratory according to a Milli-Q® system (Merck Millipore, Darmstadt, Germany). Chloroform was procured from Carlo Erba reagents (Milano, Italy). The 1-ethyl-3-(3-dimethyl aminopropyl) carbodiimide (EDC), dithiothreitol (DTT), L-glutathione reduced, and IgG from sheep serum were purchased from Sigma Aldrich. The 3,3-dithiobis (propanoic hydrazide) (DTP) was previously synthesized according to Vercruysse *et al.* [22]. The phosphate-buffered saline (PBS) used for the experiments is based on the 150 mM buffer solution at pH 7.4 of NaCl (136.9 mM), KH_2PO_4 (1.8 mM), KCl (2.7 mM), and Na_2HPO_4 (10.0 mM). The composition for the high ionic strength medium is based on the 300 mM solution at pH 7.4 of NaCl (285.5 mM), KH_2PO_4 (1.8 mM), KCl (2.7 mM), and Na_2HPO_4 (10.0 mM).

2.2. Synthesis of thiolated hyaluronic acid

The thiolated hyaluronic acid (HA-SH) was synthesized according to the study by Shu *et al.* with very slight modifications [23]. Hyaluronic acid with an average molecular weight of 38 kDa was selected for this study, as lower molecular weight variants are better suited for the development of injectable delivery systems due to their reduced viscosity, which facilitates ease of administration. Moreover, lower molecular weight hyaluronic acid offers greater accessibility for chemical modification on the polymeric chains, thereby enhancing the efficiency of functionalization processes [24,25]. The synthetic route of HA-SH synthesis is depicted in Scheme 1. Briefly, hyaluronic acid (HA, 0.005 mmol) was coupled with DTP by carbodiimide chemistry first, and then the disulfide bonds were reduced by DTT to obtain free thiol groups as terminal groups of HA pending side chains. The number of thiol groups substituted per 100 disaccharide units is defined as the substitution degree (DS). Based on the aimed DS, both HA and DTP were dissolved in 100 mL of ultrapure water at room temperature, using the ratios of 0.205 mmol, 0.671 mmol, and 1.178 mmol for DS30, DS50, and DS70, respectively. After complete dissolution, the pH of the reaction was adjusted to 4.75 by adding 1 M hydrochloric acid (HCl) solution. Subsequently, 1-ethyl-3-(3-dimethylaminopropyl) carbodiimide (EDC) was added as a carboxyl activating agent for the coupling of primary amines of HA to yield amide bonds with DTP (final ratio EDC:DTP was constantly 1:1). The pH of the reaction mixture was monitored and maintained at pH 4.75 by adding 1 M HCl solution. The reaction was stirred at room temperature for 48 h and then stopped by increasing the pH to 7 with 1 M sodium hydroxide (NaOH) solution. Afterwards, DTT (5.28 mmol) was added as a reducing agent and the pH was increased to 8.5. The reaction was carried out for a further 24 h and stopped by changing the pH to 3.5 with 1 M HCl solution. The reaction solution was transferred to a dialysis tube (Mw cutoff of 12–24 kDa) against a 100 mM sodium chloride (NaCl) solution, at 4 °C for 3 days, then dialyzed against deionized water for an additional 24 h. The final products were isolated as a dry powder by lyophilization and stored at −20 °C. The DS % was characterized by ^{1}H NMR in D_2O.

2.3. Proton nuclear magnetic resonance spectroscopy (^{1}H NMR)

The chemical structures of the synthesized polymers were characterized by proton nuclear magnetic resonance (^{1}H NMR, Varian Mercury plus 400, Crawley, UK) using deuterium oxide (D_2O) as solvent. Chemical shifts were referred to as the solvent peak (δ = 4.79 ppm for D_2O).

2.4. Hydrogel preparation

The anionic polysaccharidic hydrogels were prepared at a concentration of 15 % w/v by dissolving 15 mg of the polymers DS30, DS50 and DS70 in 100 μL of 150 mM of PBS pH 7.4 (composition in section 2.1). The polymers were stored in the incubator at 37 °C overnight to allow the gelation of the chemically crosslinked network following the

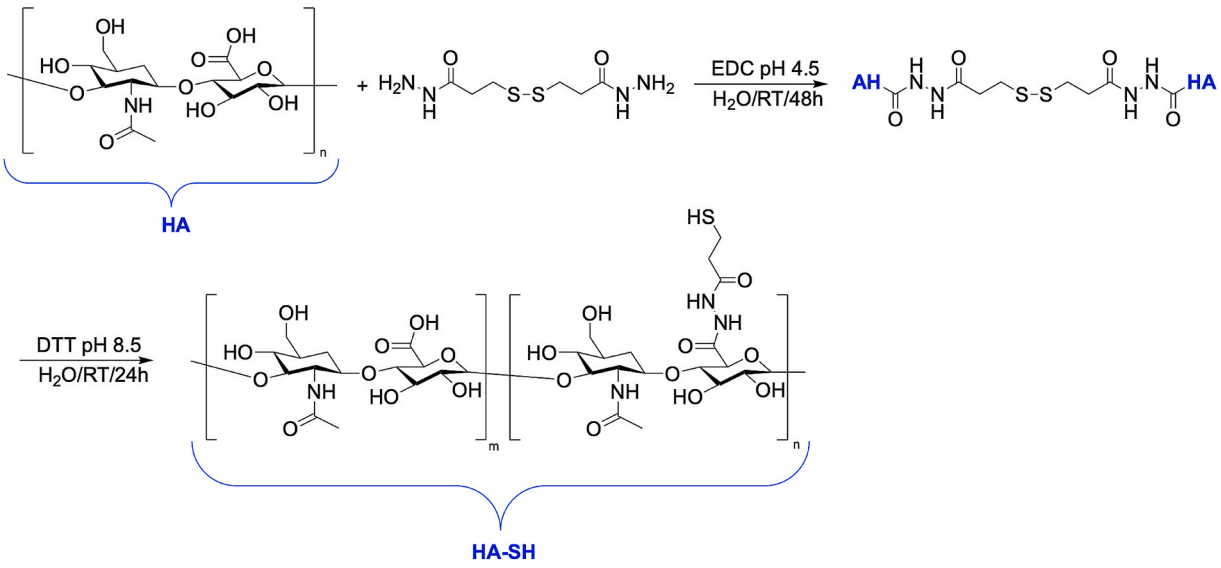

Scheme 1. Synthesis scheme of thiolated hyaluronic acid (HA-SH).

disulfide bond formation.

2.5. Swelling behavior and degradation studies

For swelling and degradation studies, 400 μL of 150 mM PBS buffer at pH 7.4 was added on top of 100 μL empty HA-SH gels (W_0), prepared according to the described procedure in section 2.4. At regular intervals, the weight of the gel upon removal of excess buffer was measured (W_t) to calculate the swelling ratio (SR = W_t/W_0) as the ratio between the weight of the gel at different time points (W_t) and the initial gel weight (W_0). After each measurement, 400 μL of fresh buffer was added on top and the vials were stored again in the incubator at 37 °C. Swelling studies for redox-response evaluation were conducted following the same procedure described before, supplementing the 150 mM PBS buffer solution (pH 7.4) with 10 mM of L-glutathione reduced (GSH), chosen as the reducing agent simulating the reduction behavior present in TME [26].

2.6. Scanning electron microscope (SEM)

The morphology of the hydrogels, for HA-SH DS30, DS50 and DS70 (formulation described in section 2.4), was evaluated by a field emission-scanning electron microscope (SEM Zeiss Sigma 300, Zeiss, Germany). The SEM sample stage was prepared by placing double-sided adhesive carbon tape on an aluminium stub. For this, first the HA-SH polymers were dissolved in MilliQ water at the concertation of 15 % w/v (aiming for a final volume of 10 μL approximately) and the solution was stored at 37 °C until complete hydrogel formation. Then, the hydrogel was placed on the sample stage and then dried at 37 °C for 48 h. Afterwards, the dried sample was sputtered under vacuum with a chromium layer of approximately 100 Å thickness (Quorum Q150T ES, Quorum Technologies, Lewes, UK) before analysis.

2.7. Rheological studies of the hydrogels

The rheological analysis of the anionic polysaccharidic hydrogels was performed on the rheometer Anton Paar MCR92 (Modular Compact Rheometer 92, Graz, Austria). HA-SH with DS30, DS50 and DS70 at a concentration of 15 % w/v (hydrogel formation described on section 2.4) were prepared in 150 mM PBS at pH 7.4 and placed on the lower plate of the instrument. The geometry system used in the study was plate-plate, with a zero-gap fixed at 0,1 mm. Viscosity analysis and frequency sweep tests were operated on the samples at a temperature of 37 °C (while oscillatory model tests can be found in the Supporting Information). For the viscosity analysis, a shear-rate-controlled test was conducted using ascending logarithmic steps to study the viscosity behavior. Viscosity was measured as a function of applied shear rate from 0.1 to 100 1/s.

Furthermore, the hydrogels were subjected to the frequency sweep test to study the change in their viscoelastic behavior with varying angular frequencies from 0.1 to 100 rad/s at a constant oscillating shear strain of 1 %.

Rheology analyses were also employed to estimate the average mesh size (ξ) of hydrogels in their hydrated state. The mesh size, measured in nanometers (nm), represents the distance between crosslinking points within the polymer network [27]. This parameter can be determined using rubber elastic theory (RET) with the following Equation (1):

$$\xi = \left(\frac{G' N_A}{RT}\right)^{-1/3} \quad (1)$$

where G' is the storage modulus, R represents the universal gas constant (8.314 J/K mol), T is the absolute temperature (310 K) and N_A denotes Avogadro constant (6.022×10^{23}) [28,29].

Another important structural property of hydrogels is the crosslinking density (ν_e) which indicates the number of elastically active junctions per unit volume (mol/m^3). This parameter can also be derived using RET, as shown in the Equation (2) below:

$$\nu_e = \frac{G_e}{RT} \quad (2)$$

where G_e corresponds to the plateau storage modulus obtained from frequency sweep tests [30]. Furthermore, rheological analysis can provide insights into the molecular weight of polymer chains between adjacent crosslinking points (M_c, measured in kg/mol). This value can be determined using the following Equation (3):

$$M_c = \frac{c\rho RT}{G_e} \quad (3)$$

where c represents the polymer concentration (15 % w/v), ρ is the density of water at 310 K (993 kg/m^3) [31].

2.8. In vitro evaluation of hydrogel biocompatibility

To assess the cell viability of the HA-SH hydrogels (DS30, DS50 and DS70), cells derived from connective mouse tissue were used. More

specifically, NCTC clone L-929 mouse fibroblasts cell line (CCL-1-ATCC, LGC Standards SrL, Milano Italy), which can be used for toxicity testing [32,33], were grown on coverslips in Eagle' Minimum Essential Medium (EMEM; ATCC, LGC Standards SrL, Milano Italy), supplemented with 10 % of Fetal Bovine Serum (FBS), penicillin and streptomycin at standard conditions (37 °C, 5 % CO_2) for four days. Then, a 15 % w/v concentration of the hydrogels DS30, DS50 and DS70 (hydrogel preparation described on section 2.4) were added on top of the cells, in the corner of the well, and incubated for an additional 24 h. Next, cultures were rinsed with phosphate saline buffer (150 mM PBS, pH = 7.4), fixed in 4 % paraformaldehyde (PFA) diluted in Dulbecco's PBS and stained with 5 % toluidine blue staining. Subsequently, cultures were observed using a Leica DM 2500 optical microscope.

Fibroblasts growth and viability in presence of hydrogels was also evaluated by MTS (3-(4,5-dimethylthiazol-2-yl)-5-(3-carboxymethoxyphenyl)-2-(4-sulfophenyl)–2H-tetrazolium) assay. Specifically, L-929 cells were plated at a density of 5′000 cells/well on DS30, DS50 and DS70 HA-SH hydrogels coated 96 well culture plates (Euroclone, SpA, Milano, Italy) or on uncoated plates (control). After 4 days of cultures, fibroblasts were incubated with 20 μL/well of Cell Titer 96 Aqueous One Solution Reagent (Promega Italia s.r.l., Milano, Italy) for 2 h in a humidified, 5 % CO_2, atmosphere. The colored formazan product resultant was measured by reading the absorbance at 490 nm using a 96-well plate reader (Tecan Italia s.r.l., MI, Italy).

2.9. IgG loading and release studies

First, immunoglobulin G (IgG) was dissolved in 150 mM PBS (pH 7.4) at a concentration of 2 mg/mL and then physically entrapped within the hydrogel network, following the methodology outlined in previous works [34–36]. The resulting solution was used for the hydrogel formulation of HA-SH DS30 and DS70 at 15 % w/v final concentration as previously described (section 2.4). After the loading of IgG within the hydrogel matrix, 900 μL of 150 mM PBS (pH 7.4) was added on top of the gels and incubated at 37 °C. At predetermined time points, 300 μL of the PBS was taken for concentration measurements, and subsequently, 300 μL of fresh buffer was replaced. To evaluate and quantify the release of IgG, High-Performance Liquid Chromatography (HPLC) analysis was performed on an HPLC-MS Agilent 1100 series (Agilent, Santa Clara, US) using a Mono Q 5/50 GL" anion exchange column (Cytiva, Marlborough, US), set at the temperature of 25 °C and a runtime of 40 min. The retention time of IgG was 20 min. The column was equilibrated in 20 mM Tris-HCL pH 7.5 and the bound material was eluted with a gradient of 0.4 M NaCl in Tris- 20 mM HCL pH 7.5.

2.10. Hydrogels thermal analyses

A differential scanning calorimeter (DSC Q2000, TA Instruments, USA) with an RCS90 refrigerated cooling system, previously calibrated with an indium standard, was employed to study the interactions between HA-SH (DS30 or DS70) and IgG. Hydrogel samples, weighing approximately 13 mg each, were placed in aluminium pans, which were then hermetically sealed. The samples were cooled to −40 °C, equilibrated for 20 min, and subsequently heated to 40 °C at a rate of 2.5 °C/min, under a nitrogen flow of 50 mL/min. The extrapolated onset melting temperature of frozen water (*T*m) was determined. The enthalpy of the solid-to-liquid transition of water was calculated by integrating the endothermic melting peak and normalizing it to the solid mass percentage of the gel [37].

2.11. Statistical analysis

The *p* values were determined by a Student's test with two-tailed distribution performed with the software GraphPad Prism 9 (GraphPad Software Inc., La Jolla, California) where p values < 0.05 are considered statistically significant.

3. Results and Discussion

3.1. ^1H NMR analysis of thiolated hyaluronic acid

Thiolated hyaluronic acid (HA-SH) is a modified form of the native polymer hyaluronic acid, which contains thiol groups (−SH) attached to its structure. This modification can significantly enhance the properties of hyaluronic acid, making it more useful for biomedical applications [18,24]. Specifically, thiolation enables the polysaccharide to become chemically cross-linkable, thereby improving its mechanical properties and providing selective degradability at specific sites, such as tumors.

The structure of HA-SH was characterized using ^{1}H NMR spectroscopy, which revealed two peaks at 2.67 ppm and 2.85 ppm corresponding to the two methylene groups adjacent to the sulfhydryl group. Additionally, the methyl group of the amide on the main chain of HA was detected at 2.03 ppm. This resonance was used as an internal standard for the calculation of the degree of substitution (DS) of the thiol group, which is in agreement with a previous study by Shu *et al.* [23]. The degree of substitution was calculated using Equation (4), which measures the ratio of the integration values at 2.67 ppm and 2.85 ppm to the integration value at 2.03 ppm (representation in Fig. 1a). The results showed an average degree of substitution of approximately 28 ± 3 %, which was considered as DS30.

$$DS = \frac{3 \times (\int (I_{2.67} + I_{2.85})}{4 \times \int I_{2.03}} \times 100 \quad (4)$$

Furthermore, a higher degree of substitution was observed in the other samples, with calculated DS values of approximately 48 ± 5 % and 69 ± 6 %, which were considered as DS50 and DS70, respectively (Fig. 1b-c). These higher degrees of substitution can be attributed to the higher integration values in the two peaks at 2.67 ppm and 2.85 ppm, indicating a higher degree of thiolation. These values are reproducible and comparable to those reported in previous studies, which ranged from 20 to 70 % for thiolated HA [25].

The degrees of substitution of 30 %, 50 % and 70 % were selected to generate three distinct hydrogel systems, enabling a comparative analysis of how variations in the modification of the HA polymeric backbone, specifically the cross-linking density, influence the physicochemical and mechanical properties of the hydrogels. The cross-linking density, defined as the number of cross-links per unit volume within the polymer network, is a crucial parameter in hydrogel design, as it directly impacts the structural integrity, mechanical strength, and diffusion characteristics of the gel [38–40]. By modulating the cross-linking density, the stability, rigidity, and ability to control the encapsulation and release of therapeutic agents can be fine-tuned, making it a key factor in optimizing HA-SH hydrogel-based delivery systems.

3.2. Swelling and degradation of hydrogels in normal versus reductive environments

The tumor microenvironment (TME) is characterized by several distinct features, including high concentrations of glutathione (GSH), acidity, hypoxia, and overexpressed enzymes and reactive oxygen species (ROS) [41]. These conditions significantly impact the behavior of hydrogels designed to interact with the TME, and the redox-responsive behavior of hydrogels is crucial for their application in tumor therapy. Previous studies have shown that the concentration of GSH in the intracellular or tumor environment is significantly higher (2–10 mM) than in the extracellular environment (2–10 μM) and elevated levels of intracellular GSH save cells from apoptosis and enhance the survival of tumor cells [42].

The abundance of GSH in the TME leads to cleavage of the disulfide bonds, which is critical for the degradation of hydrogels designed to interact with the TME. In this context, we investigated the swelling and degradation profiles of HA-SH DS30, DS50 and DS70 hydrogels in both

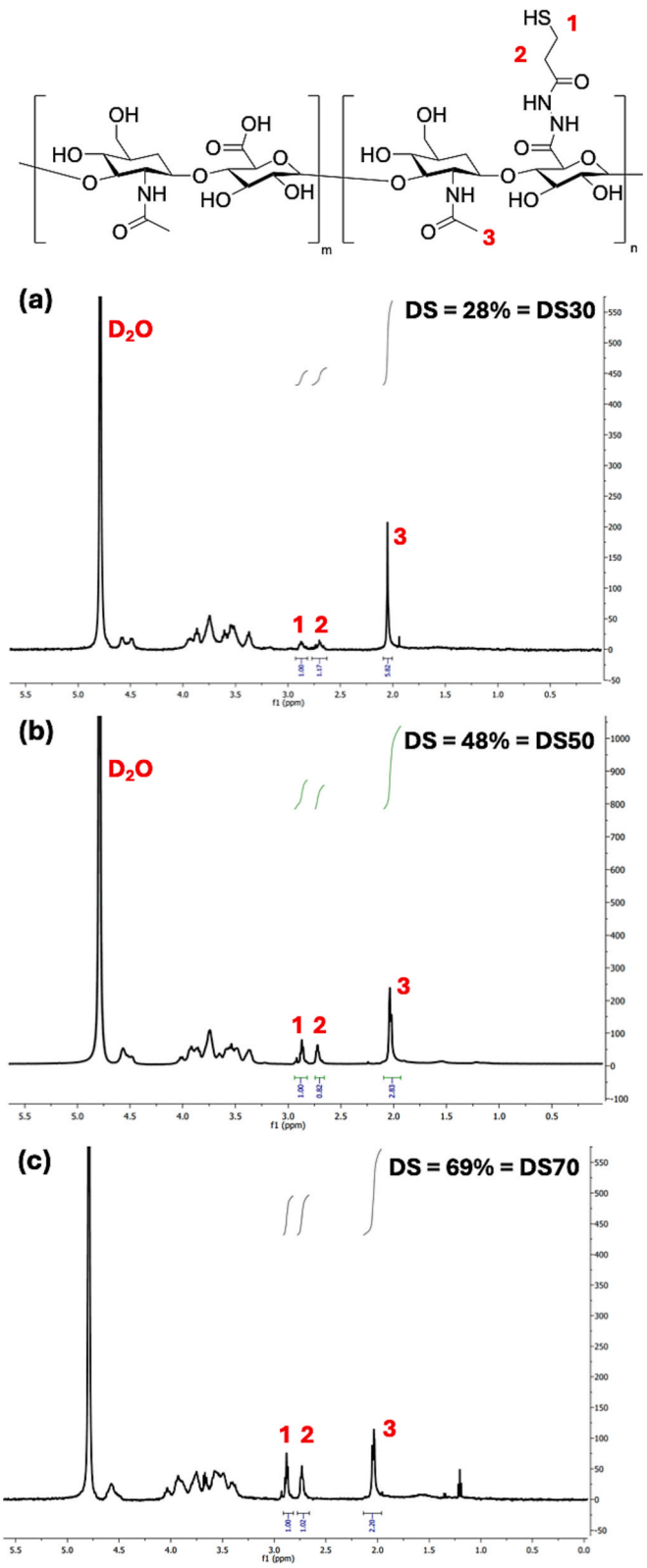

Fig. 1. Representative ^{1}H NMR spectra of HA-SH DS30 (a), HA-SH DS50 (b) and HA-SH DS70 (c) in D_2O.

physiological and reductive environments, with the latter simulated using 10 mM GSH to represent the upper range of concentrations reported in the intracellular tumor microenvironment. Fig. 2a depicts a comparison of the swelling ratio of HA-SH hydrogels in physiological (150 mM PBS, pH = 7.4), while Fig. 2b shows the degradation behaviour in a pathological medium (PBS containing 10 mM GSH to simulate the reductive TME, as proved before [43]).

DS30 gels demonstrated rapid and significant swelling in the redox environment (up to three times the initial gel weight), resulting in the complete degradation of the gels in two days. On the other hand, the swelling of the DS30 gel had a different pattern in PBS alone, where a gradual swelling of the hydrogels was observed (up to three times the initial gel weight after almost nine days) and, unlike the redox environment, the swollen gels were stable, and the gel structure was preserved for 76 days.

The observed results align with the findings of Gao *et al.*, who reported a comparable degradation behavior in a different hydrogel system [44]. Their hydrogels were formulated using native high molecular weight hyaluronic acid crosslinked with aminoethyl disulfide (AED), a glutathione (GSH)-responsive crosslinker. Under redox-active conditions, these hydrogels underwent rapid disintegration within a few days, mirroring the behavior seen in our DS30 gels, which also degraded completely within two days in a redox environment. Conversely, in non-redox environments such as distilled water, the hydrogels in Gao *et al.* study remained stable for over twenty days, similar to the DS30 gels in PBS, which exhibited gradual swelling over nine days and maintained their structural integrity for up to 76 days. These consistent findings emphasize the crucial influence of the redox state of the environment on hydrogel stability across various formulations.

In the case of HA-SH DS50 and DS70 formulations, the hydrogels exhibited a significantly lower swelling ratio than DS30 hydrogels in PBS (Fig. 2a), attributed to their higher crosslinking density and more compact structure, as highlighted in the SEM images and rheological analysis (sections 3.3 and 3.4). Additionally, DS50 and DS70 hydrogels required a longer period compared to DS30 gels before degradation and weight loss occurred in PBS, with degradation observed after 110 and 238 days, respectively. Conversely, in a reducing environment with PBS supplemented with 10 mM GSH (Fig. 2b), both DS50 and DS70 hydrogels displayed delayed swelling, reaching up to three and two times their initial gel weight, respectively, with degradation occurring after 17 and 144 days.

Overall, a distinct difference was observed in the degradation profiles of gels in PBS versus the PBS + GSH environment, confirming the redox-responsive behavior of the HA-SH hydrogel systems. This novel finding highlights the tunable nature of these hydrogels, allowing precise control over release, swelling, and degradation time by adjusting the DS to meet specific therapeutic requirements.

3.3. Morphological studies

The scanning electron microscopy (SEM) analysis of the hydrogel networks provides valuable insights into their structural properties and potential drug release behavior [45,46]. As previously reported in numerous studies, the average pore size of hydrogels is highly dependent on the crosslinking density [47,48]. Highly crosslinked hydrogels exhibit smaller pores, while less cross-linked hydrogels display larger pore sizes [49]. These porous networks can facilitate the easy flow and release of loaded drugs. However, it is important to note that the release of loaded drugs from hydrogels is not always fully dependent on the pore size, but on many other factors including the properties of both drug and the hydrogels network, and the interactions between the drug and the polymeric chains of hydrogels.

Fig. 3a shows the SEM images of the dehydrated hydrogel network of HA-SH DS30. As can be observed, the mesh size of the dehydrated hydrogel network is overall above 100 nm. In contrast, Fig. 3b-c shows the HA-SH DS50 and DS70 dehydrated hydrogels, where their mesh size is smaller than 100 nm due to increased cross-linking. Additionally, the HA-SH DS70 dehydrated hydrogel exhibits a denser network structure compared to DS30 and DS50, which is attributed to the higher degree of crosslinking. Furthermore, the SEM analysis of degraded hydrogels after exposure to PBS + GSH reveals collapse and network destruction,

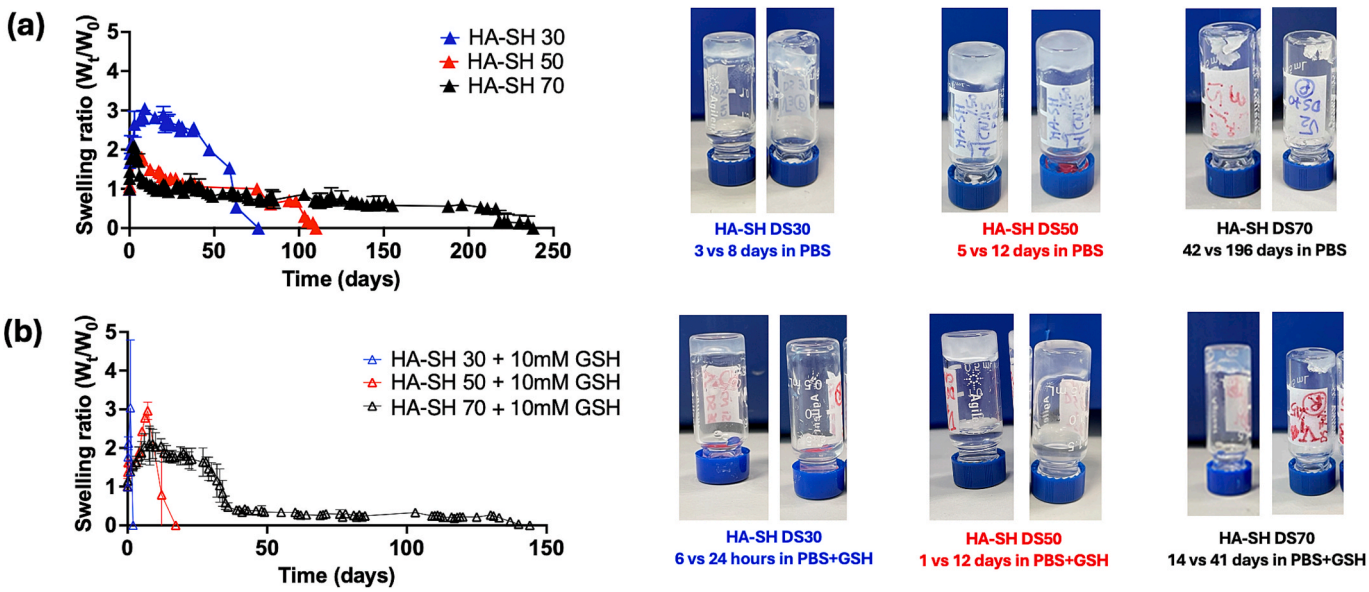

Fig. 2. Swelling ratio of HA-SH DS30, HA-SH DS50 and HA-SH DS70 (a) in physiological (150 mM PBS, pH = 7.4) and (b) in reductive environments (10 mM GSH, pH = 7.4). All values expressed as mean ± SD (n = 2–3). On the right panels representative digital images of the hydrogels at different time points.

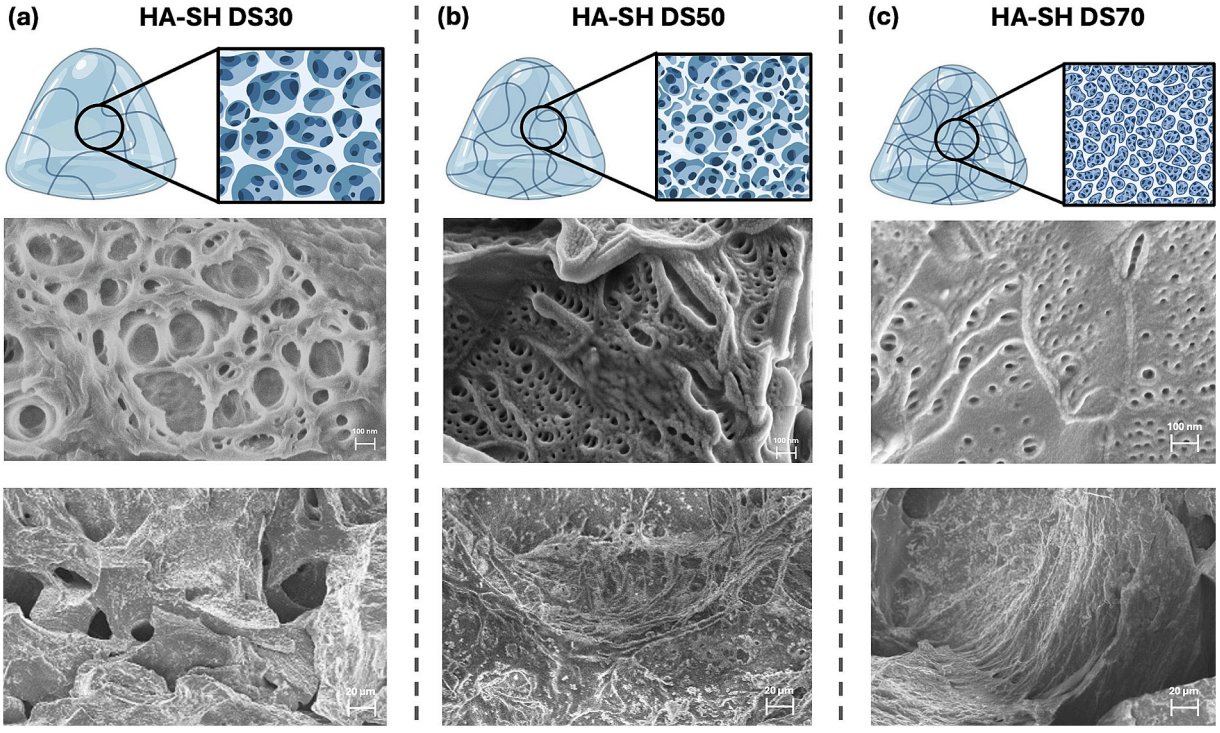

Fig. 3. (a) Graphical representation of HA-SH DS30 pores (partially created with Biorender.com); SEM analysis of the dehydrated hydrogel; SEM images of the degraded hydrogel after one day in PBS + GSH. (b) Graphical representation of HA-SH DS50 pores; SEM analysis of the dehydrated hydrogel; SEM images of the degraded hydrogel after 17 days in PBS + GSH. (c) Graphical representation of HA-SH DS70 pores; SEM analysis of the dehydrated hydrogel; SEM images of the degraded hydrogel after 144 days in PBS + GSH. Scale bars: 100 nm for dehydrated hydrogel, 20 μm for degraded hydrogel.

following the degradation time points recorded in the swelling and degradation studies (section 3.2). This observation suggests that the hydrogel network undergoes degradation and structural collapse over time when incubated with GSH at a concentration of 10 mM and is in line with the results of the degradation behavior reported in the swelling studies described before. Similarly, another study highlights how adjusting the chitosan/α,β-glycerophosphate ratio in hydrogels can fine-tune their gelation temperature, pore structure, and degradation rate, further emphasizing the crucial role of compositional tuning indicating the performance of hydrogel systems [50]. This reinforces the idea that hydrogel properties can be precisely modulated to meet specific therapeutic and structural requirements.

It is important to note that, since SEM analysis requires the hydrogels to be in a dehydrated state, the dehydration process may influence their structure and alter the observed morphology. To account for this limitation and gain a more comprehensive understanding of the hydrogels

structural and mechanical properties, rheological analysis was conducted in their native hydrated state (section 3.4). This complementary approach provides valuable insights into the hydrogels behavior under physiological conditions, offering a more complete characterization of their properties in both dry and hydrated states.

3.4. Rheological studies

The viscoelastic properties of hydrogels, such as DS30, DS50 and DS70 HA-SH gels, are critical for their application as delivery systems in cancer immunotherapy. One of the most common rheological tests for understanding the general rheological properties of hydrogels is the viscosity test, measuring the viscosity changes of the hydrogels under increasing shear rate [51]. As demonstrated in Fig. 4a, the viscosity of DS30, DS50 and DS70 hydrogels decreased with the increment of the shear rate confirming the shear thinning behavior of all systems [52]. More in detail, the viscosity values of the DS30 hydrogels started with 6205 mPa.s, decreasing to 12 mPa.s by increasing the shear rate to 100 (1/s). In the case of DS50 hydrogels, the viscosity value started at 7923 mPa.s and decreased to 59 mPa.s at 100 (1/s), indicating an intermediate viscosity profile between DS30 and DS70. For DS70 hydrogels, the viscosity value started at 42505 mPa.s and decreased to 376 mPa.s throughout the shear rate increment to 100 (1/s). The consistently higher viscosity values of DS70 hydrogels compared to DS30 and DS50 can be attributed to the higher cross-linking density and more compact structure of the DS70 hydrogels, as also demonstrated with the SEM studies (section 3.3). This increased cross-linking density results in a more robust network that resists deformation, thereby exhibiting higher viscosity [53]. Overall, this non-Newtonian behavior is characteristic of many polymeric and hydrogel systems, where the alignment of polymer chains under shear leads to a reduction in resistance to flow. Indeed, the observed shear-thinning behavior and the differences in viscosity among DS30, DS50 and DS70 hydrogels align with findings reported in previous studies. For instance, similar trends have been documented in the rheological characterization of other hydrogel systems, where increased cross-linking density correlates with higher initial viscosity and more pronounced shear-thinning behavior. Park *et al.* investigated the effects of cross-linking density on the rheological properties of gelatin-based hydrogels. They found that hydrogels with higher cross-linking densities exhibited higher viscosities and more significant reductions in viscosity under shear, which is consistent with our findings for DS70 hydrogels [54]. Furthermore, Zhou *et al.* studied the rheological and mechanical properties of cross-linked polyvinyl alcohol (PVA) hydrogels and demonstrated that increasing the cross-linking density resulted in higher viscosity and enhanced shear-thinning behavior [55]. Also, in a study by Shimojo *et al.* the effects of cross-linking density on rheological and swelling properties of hyaluronic acid hydrogels were discussed. It was observed that higher crosslinking resulted in an increment of viscosity and reduced swelling ratio [56]. All these studies support our observations regarding the DS50 and DS70 hydrogels, highlighting the importance of cross-linking density in modulating the rheological properties of hydrogel systems.

The important features of HA-SH gels highlighted by the rheology are essential for the mechanical properties and *in situ* gelification characteristics of the system, enabling minimally invasive administration [57].

The frequency sweep test was conducted to evaluate the viscoelastic properties of DS30, DS50 and DS70 hydrogels, as illustrated in Fig. 4b. The results indicate that for DS30, DS50 and DS70, the storage modulus (G′) consistently exceeds the loss modulus (G″) across the entire frequency range, confirming the gel-like characteristics of both systems. Specifically, the storage modulus of DS70 is measured at 1.1 × 10^5 Pa at an angular frequency of 0.1 rad/s, with a corresponding loss modulus of 6.6 × 10^4 Pa. Notably, both moduli demonstrate an increasing trend with rising frequency, culminating in a G′ of 2.39 × 10^5 Pa and a G″ of 1.16 × 10^5 Pa at 100 rad/s. In contrast, DS30 exhibits a storage modulus of 99,758 Pa and a loss modulus of 29,186 Pa at the same angular frequency, with both moduli decreasing to 12,221 Pa and 2973 Pa, respectively, at 100 rad/s. DS50, on the other hand, displayed intermediate mechanical properties, with a storage modulus of 4.1 × 10^4 Pa and a loss modulus of 2.5 × 10^4 Pa at an angular frequency of 0.1 rad/s, increasing to 1.1 × 10^5 Pa and 4.4 × 10^4 Pa, respectively, at 100 rad/s. Furthermore, the consistently higher storage and loss moduli of DS70 compared to DS30 and DS50 indicate a denser structure attributed to the increased cross-linking density of the former [58]. This is particularly relevant for immunotherapy applications, where the mechanical stability of the hydrogel can influence the sustained release of therapeutic agents, such as monoclonal antibodies or immune checkpoint inhibitors. This observation aligns with findings from previous studies, which have demonstrated that an increase in cross-linking density correlates with enhanced storage and loss moduli in hydrogel systems [59,60]. For example, the study performed by Wang *et al.*, demonstrates that enzymatically cross-linked peptide hydrogels exhibit denser networks and improved mechanical strength. They showed controlled release of doxorubicin, resulting in higher anticancer efficacy compared to doxorubicin solution alone [61].

Furthermore, the mesh size (ξ), crosslinking density (n_e), and average molecular weight (M_c) of the hydrogels were determined based on rheological measurements (following the equations described on section 2.7). The results showed that the mesh size decreased as the storage

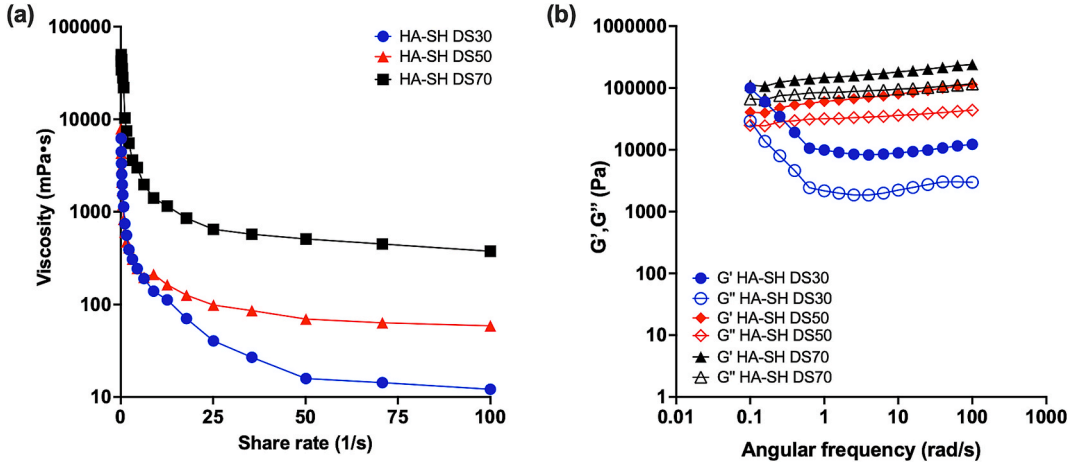

Fig. 4. (a) Viscosity tests of the HA-SH DS30, HA-SH DS50 and HA-SH DS70 hydrogels; (b) Storage (G′) and loss (G″) moduli at 37 °C as a function of frequency of the HA-SH DS30, HA-SH DS50 and HA-SH DS70 hydrogels at pH 7.4.

modulus (G′) increased, indicating a denser network structure with higher crosslinking. Conversely, the crosslinking density (n_e) increased with increasing G′, suggesting a greater number of elastically active junctions per unit volume. For gel DS30, the calculated mesh size was ~ 7.56 nm, the crosslinking density was 3.84 mol/m^3, and the average molecular weight between crosslinks was 38.8 kg/mol. As G′ increased in DS50 gel, the mesh size decreased to ~ 4.14 nm, while the crosslinking density increased to 23.45 mol/m^3, and the average molecular weight rose significantly to 6.4 kg/mol. Finally, for gel DS70, the mesh size further decreased to ~ 3.07 nm, the crosslinking density reached 57.11 mol/m^3, and the average molecular weight dropped to 2.6 kg/mol. These trends indicate that higher G′ values correlate with a more compact and crosslinked network, reducing the distance between crosslinking points and increasing the structural rigidity of the hydrogels. The decrease in M_c with increasing G′ for DS70 suggests that a greater number of shorter polymer chains exist between crosslinks, further reinforcing the hydrogel matrix. Moreover, the viscoelastic properties of these hydrogels play a pivotal role in their interaction with the TME. The ability of hydrogels to maintain structural integrity while allowing for the diffusion of therapeutic agents is crucial for effective immunotherapy. For instance, the differential viscoelastic behavior observed among DS30, DS50 and DS70 suggests that the last two may be more suitable for applications requiring prolonged residence time of the hydrogel in the site of the tumor environment, which is essential for overcoming the immunosuppressive conditions often present in tumors. Conversely, the more flexible nature of DS30 may be advantageous for injectable formulations that need to adapt to various anatomical sites within the tumor.

3.5. Hydrogels biocompatibility

The design of stimuli-responsive and biodegradable hydrogels in this study aims to utilize them as biomaterials for the delivery of immunotherapeutic agents. Therefore, evaluating the biocompatibility of these hydrogels is crucial. Biocompatibility assessments are essential to determine whether the hydrogel materials are compatible with biological systems, minimizing adverse reactions such as inflammation or tissue damage [62]. This information is vital for designing hydrogel-based therapies, including drug delivery systems aimed at cancer therapy, by interacting harmoniously with the body without damaging the healthy tissues.

To assess the biocompatibility of the DS30, DS50 and DS70 hydrogels, toluidine blue assay was used to evaluate the proliferation and growth of fibroblasts upon exposure to these hydrogels. Fig. 5a-b shows the fibroblasts growth and adhesion on plates containing DS30, DS50 and DS70 hydrogels and a hydrogel-free well used as control. The morphological characteristics and capability of expansion of fibroblast growth in the presence of hydrogels, seated at the bottom of the plate (light blue staining with pink dash lines) demonstrate that the proliferation of the fibroblast in the hydrogel environment was enhanced (Fig. 5b). Furthermore, no significant differences in cell viability were found between hydrogels fibroblasts and control cultures, rather a positive trend of cells grown on hydrogels has been detected (Fig. 5c).

The capability of the hydrogel network to positively influence cell proliferation can be attributed to the presence of hyaluronic acid. The positive effect of hyaluronic acid in proliferation and cell growth has been seen in numerous other studies, emphasizing the role of hyaluronic acid in accelerating cell growth and proliferation in various cell types [63,64]. This is consistent with the findings of previous studies that have demonstrated the biocompatibility and biodegradability of thiolated hyaluronic acid-based hydrogels [65]. The biocompatibility and biodegradability of these hydrogels make them promising biomaterials for the delivery of immunotherapeutic agents in cancer therapy.

3.6. IgG release studies

After demonstrating the redox-responsive behavior of HA-SH hydrogel systems (sections 3.2 and 3.3) and evaluating the cytocompatibility of the platforms (section. 3.5), the release profiles of IgG from HA-SH hydrogels were investigated. For this purposes, HA-SH hydrogels with DS30 and DS70 were selected as two extreme DS variants due to their distinct properties, and IgG was used as a model drug for immunotherapeutic agents in cancer treatment [66,67]. A continuous release of IgG was observed for all hydrogel formulations (Fig. 6), with release kinetics varying based on the DS of the HA-SH gel composition. As shown in Fig. 6a, the DS70 hydrogels demonstrated a

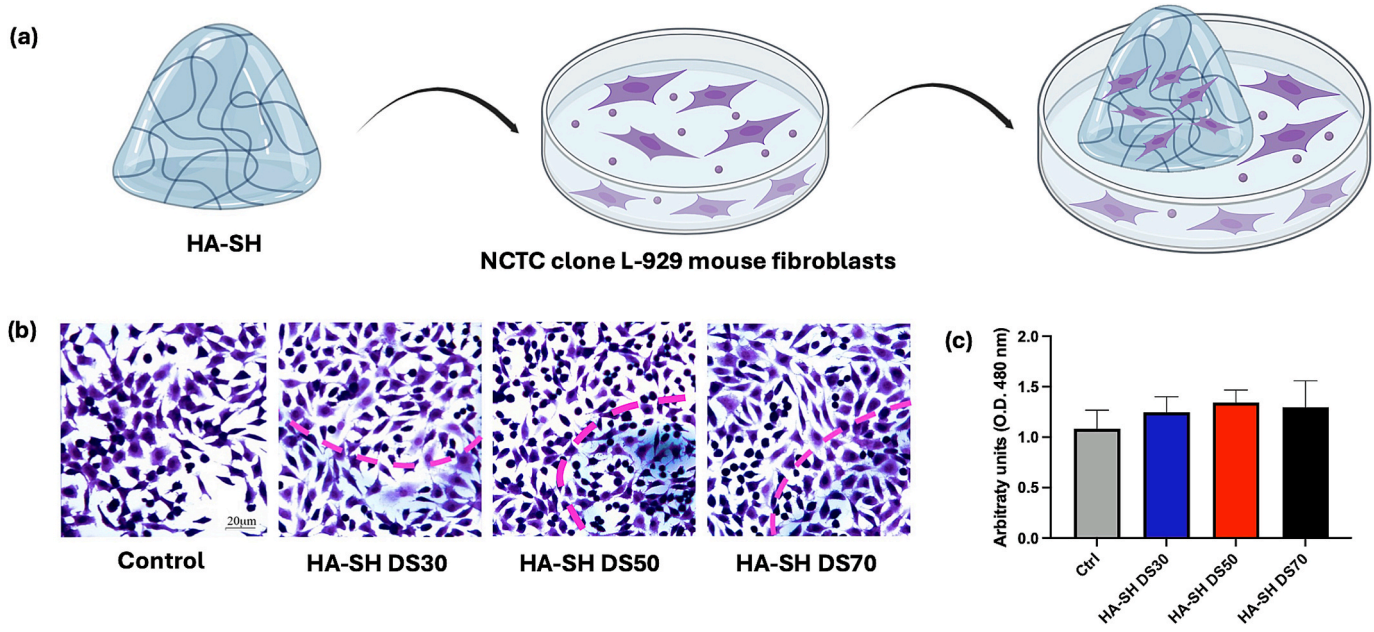

Fig. 5. Cell viability studies of the HA-SH hydrogels with NCTC clone L-929 mouse fibroblasts. (a) Schematic representation of the *in vitro* experiment. Scheme was partially created with Biorender.com; (b) Fibroblast adhesion and growth in DS30, DS50 and DS70 hydrogels (control was included as fibroblasts in a gel-free well), scale bar = 20 μm. (c) Cytocompatibility of DS30, DS50 and DS70 hydrogels investigated following the MTS assay (n = 3, mean ± SD).

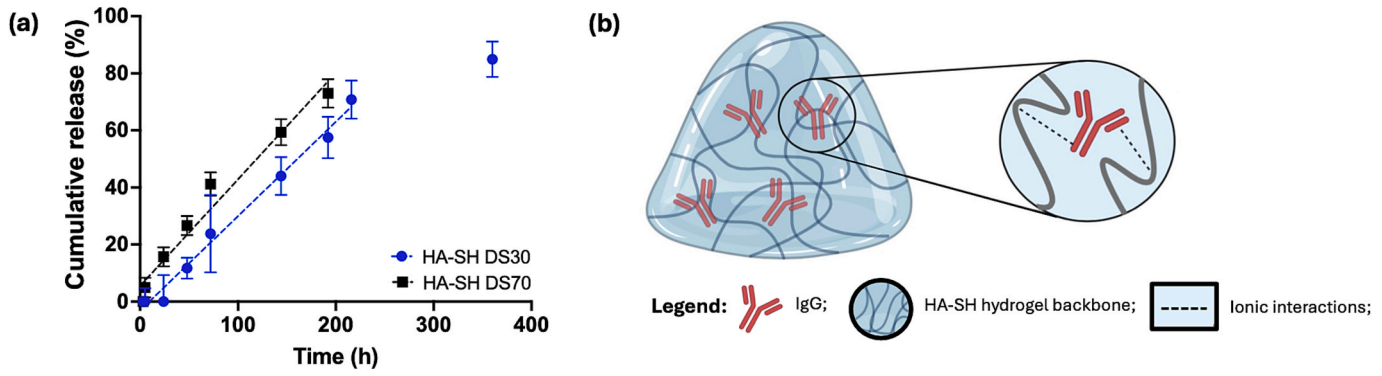

Fig. 6. (a) IgG cumulative release profile of DS30 and DS70 hydrogels at pH 7.4 (150 mM PBS) and 37 °C (n = 2, mean ± SD); (b) Graphical representation of the ionic interactions between the HA-SH gel backbone and the IgG. Scheme was partially created with Biorender.com.

fast release of IgG in the first few hours, followed by a linear trend leading to a cumulative release of 73 %, whereas in DS30 hydrogels the release initiated after two days and prolonged for twelve days with a cumulative release of almost 85 %.

The release mechanism of IgG from the HA-SH hydrogels was examined by fitting the release curve to the Ritger-Peppas equation (5):

$$\frac{M_t}{M_\infty} = kt^n \quad (5)$$

Here, the fractional release of the loaded drug is represented, k is a kinetic constant, t is the release time, and n is the diffusional exponent, which is closely related to the release mechanism of the drug. If $n = 0.5$, the release is governed by Fickian diffusion; if $n = 1$, the molecules are released by surface erosion; and if n has a value between 0.5 and 1, both mechanisms are involved [68].

In this case, the experimental release curves of both DS30 and DS70 fitted to n-value of 1. Therefore, the release studies revealed that Ig G is released in a zero-order kinetics manner from both HA-SH hydrogels. Structurally, IgG has dimensions of approximately 14.5 nm in length, 8.5 nm in width, and 4.0 nm in thickness, with antigen-binding sites separated by about 13.7 nm [69]. These structural dimensions are consistent with the hydrodynamic measurements, considering that the

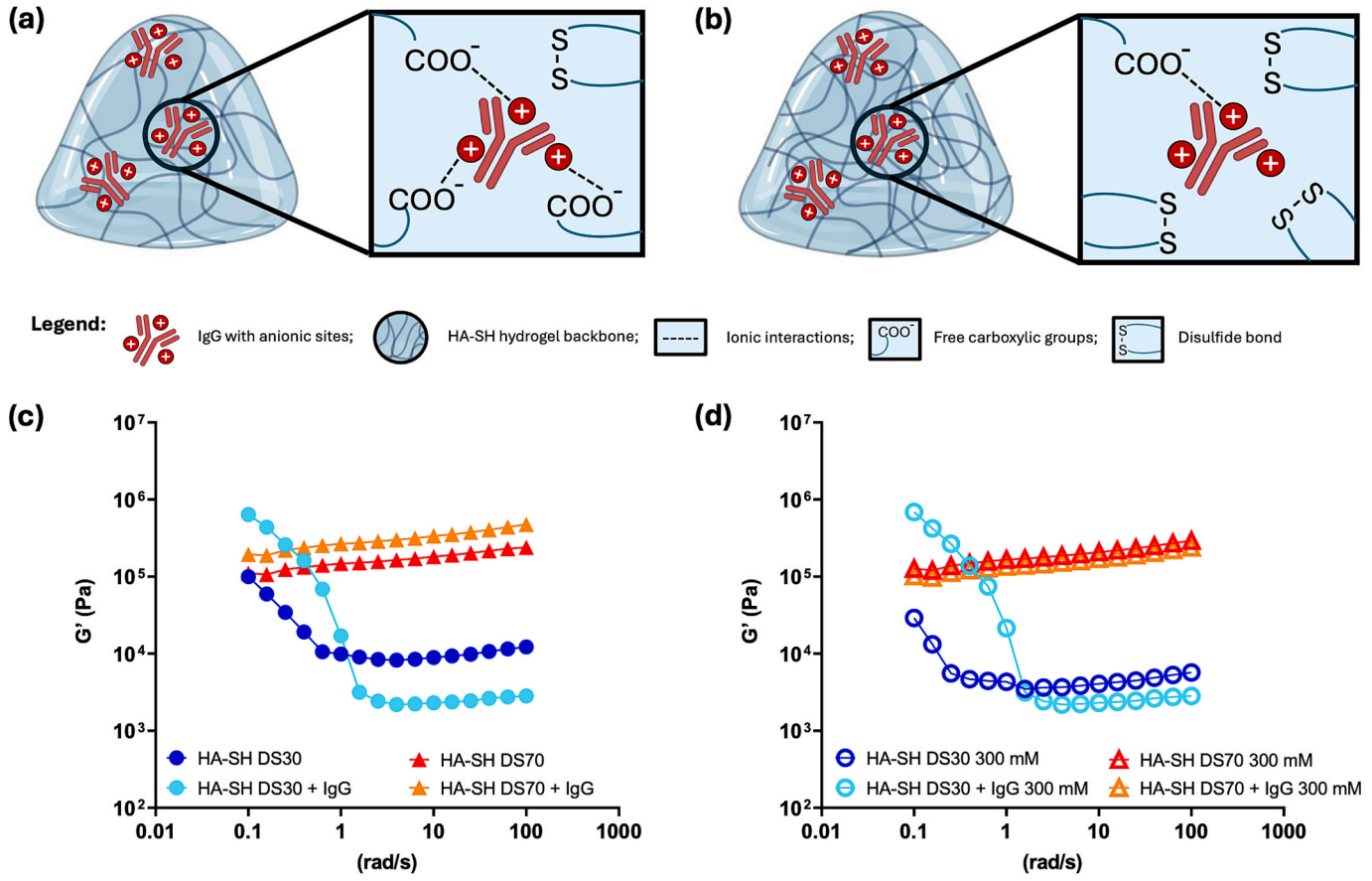

Fig. 7. Proposed mechanism of ionic interaction between positive charge(s) of IgG with HA-SH DS30 (a) and DS70 (b). Scheme was partially created with Biorender.com. For a better understanding of the mechanism, IgG was depicted with positive sites to highlight its interaction with the anionic portions of HA. However, as mentioned in the main text, IgG has a polycharged nature with a slightly negative net charge. Rheological measurements of HA-SH DS30 and DS70 placebo and IgG-loaded hydrogels showing storage modulus as a function of frequency at 37 °C, pH 7.4, in 150 mM (c) and 300 mM (d) buffer conditions.

hydrodynamic size accounts for the molecule's behavior in solution, including factors like shape and solvation [70]. These findings align with the hydrated structural properties of the hydrogels discussed earlier (section 3.4), where HA-SH networks indeed possess a smaller mesh size than IgG, leading to a non-diffusional system.

However, beyond the physical constraints of the HA-SH hydrogel mesh, the release kinetics were influenced by the DS percentage of HA-SH, most notably through ionic interactions between the remaining negatively charged HA-SH polymer chains and the polycharged nature of IgG. As seen in many previous studies such as a work by Casadidio *et al.*, the interchange of the crosslinking density, charge interactions, and modification of polysaccharides can influence the release kinetics of drugs from polysaccharide-based hydrogels [37]. Therefore, also in this case the IgG release profile is not only directly related to the pore mesh size, but also to the complex ionic interactions between the charged nature of the IgG and the anionic polymeric chains of hyaluronic acid (Fig. 6b). Generally speaking, the net charge of an IgG molecule depends on the pH of the surrounding environment because proteins like IgG contain amino acids with ionizable side chains that can gain or lose protons. At physiological pH (around 7.4), the overall net charge of IgG can vary but is generally slightly negative [71]. Even though the IgG is anionic in the pH of the hydrogel network, it also possesses positive charges that can bind to the negative charges of the hyaluronic acid polymeric chain (Fig. 7a-b). Indeed, IgG molecules are composed of amino acids that can be positively or negatively charged depending on the pH, yielding to ionic interaction also with anionic sites [71]. The HA-SH DS70 has fewer negative charges due to its high DS and, therefore, fewer interactions with the IgG structure, which leads to a fast release of IgG in the first few hours. In the case of HA-SH DS30 the polymeric chains contain more negative charges that can bind with IgG, therefore, more time is needed for the unbinding and release of the IgG, leading to a delayed release initiation (after two days). To confirm this hypothesis and further investigate the role of ionic interactions, rheological measurements of IgG-loaded hydrogels were performed according to the protocol described in section 2.7. As shown in Fig. 7c, incorporation of IgG into the HA-SH DS30 hydrogel resulted in a substantial increase in the storage modulus (G′). At a frequency of 0.1 rad/s, G′ increased from approximately 100 kPa in the HA-SH DS30 placebo to about 639 kPa in the IgG-loaded hydrogel. In contrast, the effect of IgG on the rheological properties of the HA-SH DS70 hydrogel was less pronounced, with G′ increasing from 110 kPa (placebo) to 194 kPa (IgG-loaded). To further assess the influence of electrostatic interactions, control experiments were conducted under high ionic strength conditions to screen potential interactions between negatively charged HA and positively charged regions of IgG (Fig. 7d). Under these conditions (300 mM buffer, composition in section 2.1), placebo and IgG-loaded hydrogels were compared. The DS70 hydrogel did not show an increase of G′ indicating effective ionic shielding. In contrast, the DS30 hydrogel still exhibited an increase in G′ in the presence of IgG, however, the reason for this observation remains unclear. These results support the hypothesis that the positively charged domains of IgG interact electrostatically with the carboxylate ($–COO^-$) groups of the HA-SH network, thereby enhancing the mechanical properties of the hydrogel [37]. Moreover, the extent of this enhancement appears to be modulated by the DS of HA-SH, which likely influences the density and distribution of available binding sites within the network. Overall, these findings offer a comprehensive insight into the mechanisms governing IgG release from HA-SH hydrogels, demonstrating zero-order release kinetics. This controlled release is driven by a dual mechanism involving DS and structural properties of the hydrogel, as well as the poly-charged nature of IgG and its ionic interactions with the HA-SH backbone. These finding are essential for the development of hydrogel-based drug delivery systems intended for local administration, where maintaining a consistent and controlled release profile is critical.

In both cases, the cumulative release of IgG in the PBS environment does not reach full completion. This is likely due to limitations in the HPLC detection method, which may fail to capture all residual IgG present in the system. Additionally, some IgG molecules may remain entrapped within the hydrogel network due to ionic interactions or binding with the HA-SH clusters formed during the gel erosion process, as found by Liang *et al.* [72]. These interactions could hinder the complete recovery of IgG after filtration, potentially affecting the accuracy of HPLC injection measurements and leading to an underestimation of the total released protein. This phenomenon is consistent with findings by Zhang *et al.*, who observed incomplete release of bovine serum albumin (BSA) from a redox-responsive hyaluronic acid-based hydrogel, with some BSA initially trapped in the network due to similar interactions. These results suggest that a portion of the IgG in our study may likewise be retained within the hydrogel structure [66]. However, it should be noted that IgG may also be fragmented and destabilized in time and become unrecognizable by the analysis method of the drug release [73].

3.7. Thermal analysis

Thermal analysis was conducted to elucidate the influence of the degree of thiolation in HA-SH hydrogels on the release of IgG from the matrix, as already highlighted by the rheological measurements described above (Fig. 7c). Fig. 8 illustrates the onset melting temperatures (*T*m) and melting enthalpies (Δ*H*) for frozen water in the different samples at pH 7.4, comparing placebo and IgG-loaded hydrogels. The onset melting temperature results indicate notable differences between placebo and IgG-loaded samples, depending on the type of HA-SH used (Fig. 8a). For the HA-SH DS30 hydrogel, the presence of IgG significantly lowered the onset melting temperature from -3.63 ± 2.09 °C to -4.54 ± 2.62 °C, suggesting that IgG loading influences the thermal properties of the hydrogel, potentially due to the ionic interactions between the positive charges of IgG with the unmodified carboxyl groups of HA-SH DS30. This observation supports the idea that the presence of IgG modifies the DS30 gel behaviour, influencing its thermal properties. Conversely, the HA-SH DS70 hydrogel exhibited a minor increase in onset melting temperature when IgG was incorporated, rising from -3.88 ± 2.33 °C to -3.05 ± 2.47 °C. This trend suggests that the effect of IgG on the thermal properties of the hydrogel may depend on the DS of HA-SH. The melting enthalpy (ΔH) results for frozen water in the various HA-SH hydrogels further highlights the impact of IgG loading on the thermal properties of these materials (Fig. 8b). For the HA-SH DS30 hydrogel, the melting enthalpy decreases from 276.36 ± 2.35 J/g to 247.64 ± 1.90 J/g with the addition of IgG. This significant reduction suggests that IgG interacts with the hydrogel matrix, potentially altering the network structure and its capacity to entrap water when IgG is loaded. In the case of HA-SH DS70 hydrogels, the change in melting enthalpy with IgG loading is less pronounced, decreasing slightly from 275.85 ± 5.37 J/g to 273.8 ± 9.95 J/g. This minimal change indicates that the higher degree of substitution (DS70) might provide a more robust network that is less affected by the incorporation of IgG.

Overall, these findings suggest that the presence of IgG statistically reduces the melting enthalpy of frozen water within the HA-SH DS30 hydrogel and not in the DS70 formulations. This could be due to differences in the structural dynamics and interactions between the polymer network and the IgG molecules. As discussed in Section 3.6, the release studies indicate that HA-SH DS30 releases 71 % of the drug over 216 h, whereas HA-SH DS70 releases 73 % in just 120 h. This difference in drug release rates aligns with the rheological and thermal analysis results, suggesting a correlation among mechanical properties, thermal behavior, structural integrity, and the controlled release of IgG. These findings further support the dual release mechanism theory, which is governed by both the DS of the gel and the ionic interactions between IgG and the HA-SH backbone.

4. Conclusions

Immunotherapy has emerged as a standard treatment for various

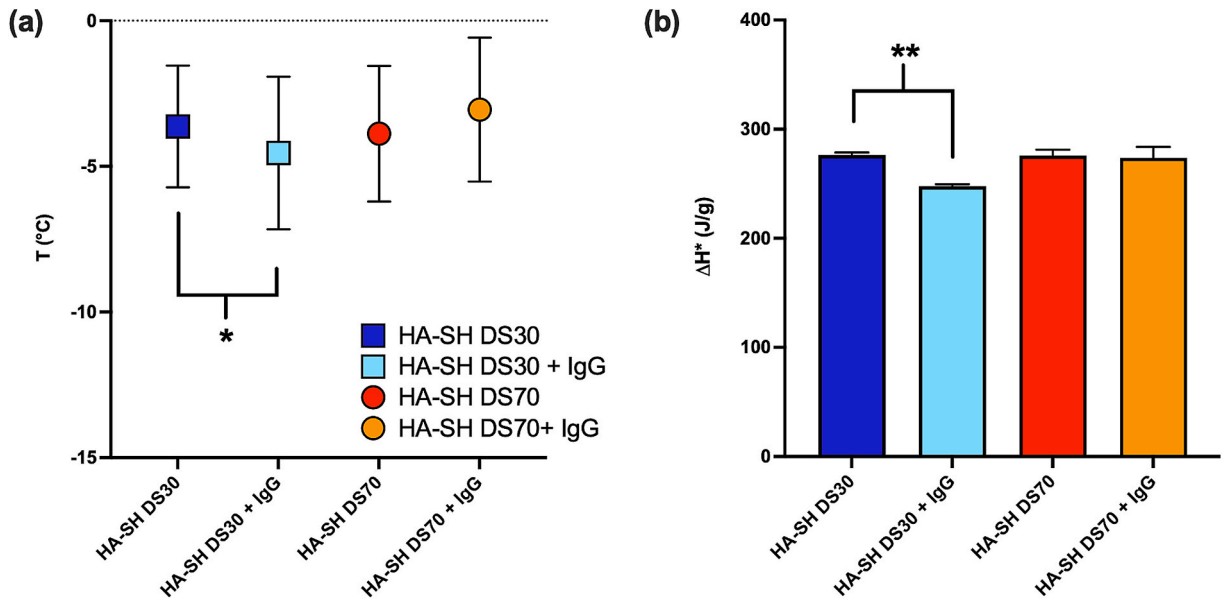

Fig. 8. Water melting temperatures (a) and melting enthalpies (b) of placebo and IgG-loaded HA-SH hydrogels at pH 7.4 (n = 2, mean ± SD). *p < 0.05, **p < 0.01.

cancers, however, its broader clinical success is often limited by challenges such as suboptimal pharmacokinetics and lack of precise tumor targeting, leading to immune-related side effects and reduced efficacy. The oxidized thiolated hyaluronic acid-based system investigated here offers a biocompatible platform that enables the controlled local release of native antibodies, addressing these limitations and enhancing therapeutic precision. These *in situ* forming HA-SH hydrogels exhibit redox sensitivity, making them particularly responsive to the reductive tumor microenvironment. This study also introduces, for the first time in this system, a dual release mechanism, explaining how drug release from these hydrogels is governed by both the DS in the HA chemical structure and the ionic interactions between IgG and the HA-SH backbone. These insights highlight the intricate interplay of physical and chemical factors that influence drug release kinetics. Specifically, DS70 hydrogels demonstrate potential for applications requiring rapid local delivery of immunotherapeutic agents, whereas DS30 hydrogels are better suited for sustained and prolonged release. Collectively, these properties support the development of novel delivery platforms designed to reduce side effects, enhance therapeutic efficacy, and be tailored to individual patient needs.

CRediT authorship contribution statement

Bita Mahdavi Firouzabadi: Writing – review & editing, Formal analysis, Writing – original draft, Conceptualization, Investigation, Methodology. **Maria Rosa Gigliobianco:** Writing – review & editing, Methodology, Conceptualization, Investigation. **Dimitrios Agas:** Methodology, Investigation, Conceptualization, Formal analysis. **Maria Giovanna Sabbieti:** Methodology, Investigation, Conceptualization, Formal analysis. **Claudio Alimenti:** Methodology, Investigation, Conceptualization, Formal analysis. **Lakshmi Sathi Devi:** Formal analysis, Writing – review & editing, Conceptualization. **Cristina Casadidio:** Investigation, Writing – original draft, Conceptualization, Methodology, Writing – review & editing, Formal analysis. **Piera Di Martino:** Conceptualization, Supervision, Funding acquisition, Writing – review & editing. **Roberta Censi:** Conceptualization, Supervision, Funding acquisition, Writing – review & editing.

Declaration of competing interest

The authors declare that they have no known competing financial interests or personal relationships that could have appeared to influence the work reported in this paper.

Acknowledgments

This research was granted by European Commission H2020-MSCA-ITN-2020-CAST (grant number 857894).

Appendix A. Supplementary data

Supplementary data to this article can be found online at https://doi.org/10.1016/j.ejpb.2025.114804.

Data availability

Data will be made available on request.

References

[1] I. Rana, et al., Nanocarriers for cancer nano-immunotherapy, Drug Deliv. Transl. Res. 13 (7) (2023) 1936–1954.
[2] E. Askari, et al., Cancer immunotherapy using bioengineered micro/nano structured hydrogels, Adv. Healthc. Mater. 12 (27) (2023) 2301174.
[3] L.S. Devi, et al., Multifunctionality of cyclodextrin-based polymeric nanoparticulate delivery systems for chemotherapeutics, combination therapy, and theranostics, Int. J. Pharm. (2024) 123976.
[4] M. Aquib, et al., Advances in local and systemic drug delivery systems for post-surgical cancer treatment, J. Mater. Chem. B 8 (37) (2020) 8507–8518.
[5] H. Wang, et al., Biomaterial-based scaffold for in situ chemo-immunotherapy to treat poorly immunogenic tumors, Nat. Commun. 11 (1) (2020) 5696.
[6] J.T. Ryman, B. Meibohm, Pharmacokinetics of monoclonal antibodies, CPT Pharmacometrics Syst. Pharmacol. 6 (9) (2017) 576–588.
[7] Y. Ma, et al., Recent advances in macroporous hydrogels for cell behavior and tissue engineering, Gels 8 (10) (2022) 606.
[8] C. Hiemstra, et al., In vitro and in vivo protein delivery from in situ forming poly (ethylene glycol)–poly (lactide) hydrogels, J. Control. Release 119 (3) (2007) 320–327.
[9] X. Tong, et al., Long-Term controlled protein release from poly (ethylene glycol) hydrogels by modulating mesh size and degradation, Macromol. Biosci. 15 (12) (2015) 1679–1686.
[10] V.H. Pérez-Luna, O. González-Reynoso, Encapsulation of biological agents in hydrogels for therapeutic applications, Gels 4 (3) (2018) 61.
[11] B. Arneth, Tumor microenvironment, Medicina 56 (1) (2019) 15.
[12] A. Lierova, et al., Hyaluronic acid: known for almost a century, but still in vogue, Pharmaceutics 14 (4) (2022) 838.
[13] S. Salathia, et al., Hyaluronic acid-based nanosystems for CD44 mediated anti-inflammatory and antinociceptive activity, Int. J. Mol. Sci. 24 (8) (2023) 7286.

[14] S. Arpicco, et al., Hyaluronic acid conjugates as vectors for the active targeting of drugs, genes and nanocomposites in cancer treatment, Molecules 19 (3) (2014) 3193–3230.
[15] S. Kim, et al., Alum-tuned hyaluronic acid-based hydrogel with immune checkpoint inhibition for immunophoto therapy of cancer, J. Control. Release 362 (2023) 1–18.
[16] J.H. Kim, et al., Hyaluronic acid-based nanomaterials for cancer therapy, Polymers 10 (10) (2018) 1133.
[17] C. Casadidio, et al., Daptomycin-loaded biodegradable thermosensitive hydrogels enhance drug stability and foster bactericidal activity against Staphylococcus aureus, Eur. J. Pharm. Biopharm. 130 (2018) 260–271.
[18] S. Tiwari, P. Bahadur, Modified hyaluronic acid based materials for biomedical applications, Int. J. Biol. Macromol. 121 (2019) 556–571.
[19] B. Mahdavi Firouzabadi, et al., Design of nanoparticles in cancer therapy based on tumor microenvironment properties, Pharmaceutics 14 (12) (2022) 2708.
[20] S. Yin, et al., Intracellular delivery and antitumor effects of a redox-responsive polymeric paclitaxel conjugate based on hyaluronic acid, Acta Biomater. 26 (2015) 274–285.
[21] D. Xia, et al., Redox/ph-responsive biodegradable thiol-hyaluronic acid/chitosan charge-reversal nanocarriers for triggered drug release, Polymers 13 (21) (2021) 3785.
[22] K.P. Vercruysse, et al., Synthesis and in vitro degradation of new polyvalent hydrazide cross-linked hydrogels of hyaluronic acid, Bioconjug. Chem. 8 (5) (1997) 686–694.
[23] X.Z. Shu, et al., Disulfide cross-linked hyaluronan hydrogels, Biomacromolecules 3 (6) (2002) 1304–1311.
[24] R. Censi, et al., Interpenetrating hydrogel networks enhance mechanical stability, rheological properties, release behavior and adhesiveness of platelet-rich plasma, Int. J. Mol. Sci. 21 (4) (2020) 1399.
[25] R. Censi, et al., Thermosensitive hybrid hydrogels for the controlled release of bioactive vancomycin in the treatment of orthopaedic implant infections, Eur. J. Pharm. Biopharm. 142 (2019) 322–333.
[26] Y. Li, et al., A simple glutathione-responsive turn-on theranostic nanoparticle for dual-modal imaging and chemo-photothermal combination therapy, Nano Lett. 19 (8) (2019) 5806–5817.
[27] J. Karvinen, et al., Characterization of the microstructure of hydrazone crosslinked polysaccharide-based hydrogels through rheological and diffusion studies, Mater. Sci. Eng. C 94 (2019) 1056–1066.
[28] P.B. Welzel, et al., Modulating biofunctional starPEG heparin hydrogels by varying size and ratio of the constituents, Polymers 3 (1) (2011) 602–620.
[29] M. Rubinstein, R.H. Colby, Oxford University Press: New York. NY, USA, 2003. 23: p. 259.
[30] R. Suriano, et al., Rheological and mechanical behavior of polyacrylamide hydrogels chemically crosslinked with allyl agarose for two-dimensional gel electrophoresis, J. Mech. Behav. Biomed. Mater. 30 (2014) 339–346.
[31] S. Piskounova, et al., The effect of mixing on the mechanical properties of hyaluronan-based injectable hydrogels, Macromol. Mater. Eng. 296 (10) (2011) 944–951.
[32] R. Zange, T. Kissel, Comparative in vitro biocompatibility testing of polycyanoacrylates and poly (D, L-lactide-co-glycolide) using different mouse fibroblast (L929) biocompatibility test models, Eur. J. Pharm. Biopharm. 44 (2) (1997) 149–157.
[33] M. Szymonowicz, et al., Cytotoxicity evaluation of high-temperature annealed nanohydroxyapatite in contact with fibroblast cells, Materials 10 (6) (2017) 590.
[34] G. Tripodo, et al., Controlled release of IgG by novel UV induced polysaccharide/poly (amino acid) hydrogels, Macromol. Biosci. 9 (4) (2009) 393–401.
[35] O. Franssen, O. Vos, W. Hennink, Delayed release of a model protein from enzymatically-degrading dextran hydrogels, J. Control. Release 44 (2–3) (1997) 237–245.
[36] C. Hiemstra, et al., Release of model proteins and basic fibroblast growth factor from in situ forming degradable dextran hydrogels, J. Control. Release 122 (1) (2007) 71–78.
[37] C. Casadidio, et al., Anionic polysaccharides for stabilization and sustained release of antimicrobial peptides, Int. J. Pharm. 636 (2023) 122798.
[38] Y. Wu, S. Joseph, N. Aluru, Effect of cross-linking on the diffusion of water, ions, and small molecules in hydrogels, J. Phys. Chem. B 113 (11) (2009) 3512–3520.
[39] T. Miyazaki, et al., In situ synthesis of magnetic iron oxide nanoparticles in chitosan hydrogels as a reaction field: effect of cross-linking density, Colloids Surf. B Biointerfaces 179 (2019) 334–339.
[40] J.S. Bermejo, C.M. Ugarte, Influence of cross-linking density on the glass transition and structure of chemically cross-linked PVA: a molecular dynamics study, Macromol. Theory Simul. 18 (6) (2009) 317–327.
[41] W. Yang, et al., Tumor microenvironment triggered biodegradation of inorganic nanoparticles for enhanced tumor theranostics, RSC Adv. 10 (45) (2020) 26742–26751.
[42] A. Bansal, M.C. Simon, Glutathione metabolism in cancer progression and treatment resistance, J. Cell Biol. 217 (7) (2018) 2291–2298.
[43] Y. Nie, et al., A glutathione-triggered precision explosive system for improving tumor chemosensitivity, Nano Res. (2021) 1–11.
[44] Z. Gao, et al., A redox-responsive hyaluronic acid-based hydrogel for chronic wound management, J. Mater. Chem. B 7 (47) (2019) 7494–7501.
[45] J.M. Urueña, et al., Mesh size control of polymer fluctuation lubrication in gemini hydrogels, Biotribology 1 (2015) 24–29.
[46] Y. Amamoto, et al., Mesh-size control and functionalization of reorganizable chemical gels by monomer insertion into their cross-linking points, Polym. Chem. 2 (4) (2011) 957–962.
[47] J.S. Varghese, N. Chellappa, N.N. Fathima, Gelatin–carrageenan hydrogels: Role of pore size distribution on drug delivery process, Colloids Surf. B Biointerfaces 113 (2014) 346–351.
[48] T. Kopač, A. Ručigaj, M. Krajnc, The mutual effect of the crosslinker and biopolymer concentration on the desired hydrogel properties, Int. J. Biol. Macromol. 159 (2020) 557–569.
[49] J. Jang, et al., Effects of alginate hydrogel cross-linking density on mechanical and biological behaviors for tissue engineering, J. Mech. Behavior Biomed. Mater. 37 (2014) 69–77.
[50] Q.F. Dang, et al., Controlled gelation temperature, pore diameter and degradation of a highly porous chitosan-based hydrogel, Carbohydr. Polym. 83 (1) (2011) 171–178.
[51] G. Stojkov, et al., Relationship between structure and rheology of hydrogels for various applications, Gels 7 (4) (2021) 255.
[52] K. Pramod, S. Shanavas, I. Baby, Rheological profiling of a hydrogel drug delivery vehicle, J. Chem. Pharm. Res. 7 (2015) 818–825.
[53] C. Seidel, et al., Influence of the cross-linking agent on the gel structure of starch derivatives, Starch-Stärke 53 (7) (2001) 305–310.
[54] H.E. Park, et al., Effect of temperature on gelation and cross-linking of gelatin methacryloyl for biomedical applications, Phys. Fluids 32 (3) (2020).
[55] Z. Zhou, et al., Effects of poly (vinyl alcohol)(PVA) concentration on rheological behavior of TEMPO-mediated oxidized cellulose nanofiber/PVA suspensions, Cellul. 29 (15) (2022) 8255–8263.
[56] A.A.M. Shimojo, et al., The crosslinking degree controls the mechanical, rheological, and swelling properties of hyaluronic acid microparticles, J. Biomed. Mater. Res. A 103 (2) (2015) 730–737.
[57] M. Guvendiren, H.D. Lu, J.A. Burdick, Shear-thinning hydrogels for biomedical applications, Soft Matter 8 (2) (2012) 260–272.
[58] D.K. Baby, Rheology of hydrogels, in: Rheology of Polymer Blends and Nanocomposites, Elsevier, 2020, pp. 193–204.
[59] D. Calvet, J.Y. Wong, S. Giasson, Rheological monitoring of polyacrylamide gelation: Importance of cross-link density and temperature, Macromolecules 37 (20) (2004) 7762–7771.
[60] X. Zhang, et al., Preparation and rheological studies on the solvent based acrylic pressure sensitive adhesives with different crosslinking density, Int. J. Adhes. Adhes. 31 (7) (2011) 760–766.
[61] X. Wang, et al., Enzymatically cross-linked peptide hydrogels for enhanced self-assembling capability and controlled drug release, New J. Chem. 47 (19) (2023) 9451–9458.
[62] R. Kilic Boz, et al., Redox-responsive hydrogels for tunable and "On-demand" release of biomacromolecules, Bioconjug. Chem. 33 (5) (2022) 839–847.
[63] J.K. Kutty, et al., The effect of hyaluronic acid incorporation on fibroblast spreading and proliferation within PEG-diacrylate based semi-interpenetrating networks, Biomaterials 28 (33) (2007) 4928–4938.
[64] Y. Lei, et al., The spreading, migration and proliferation of mouse mesenchymal stem cells cultured inside hyaluronic acid hydrogels, Biomaterials 32 (1) (2011) 39–47.
[65] X. Qin, et al., An extracellular matrix-mimicking hydrogel for full thickness wound healing in diabetic mice, Macromol. Biosci. 18 (7) (2018) 1800047.
[66] R. Zhang, et al., Preparation and properties of redox responsive modified hyaluronic acid hydrogels for drug release, Polym. Adv. Technol. 28 (12) (2017) 1759–1763.
[67] C. Pan, et al., Next-generation immuno-oncology agents: current momentum shifts in cancer immunotherapy, J. Hematol. Oncol. 13 (1) (2020) 29.
[68] P.L. Ritger, N.A. Peppas, A simple equation for description of solute release II. Fickian and anomalous release from swellable devices, J. Control. Release 5 (1) (1987) 37–42.
[69] H. Bagçi, et al., Monoclonal anti-biotin antibodies simulate avidin m the recognition of biotin, FEBS Lett. 322 (1) (1993) 47–50.
[70] Y.H. Tan, et al., A nanoengineering approach for investigation and regulation of protein immobilization, ACS Nano 2 (11) (2008) 2374–2384.
[71] D. Yang, et al., IgG charge: practical and biological implications, Antibodies 8 (1) (2019) 24.
[72] S. Liang, et al., Injectable nanocomposite hydrogels improve intraperitoneal co-delivery of chemotherapeutics and immune checkpoint inhibitors for enhanced peritoneal metastasis therapy, ACS Nano 18 (29) (2024) 18963–18979.
[73] I. Correia, Stability of IgG isotypes in serum. Mabs, Taylor & Francis, 2010.